Applied Surface Science 565 (2021) 150495

Contents lists available at ScienceDirect

Applied Surface Science

journal homepage: www.elsevier.com/locate/apsusc

Full Length Article

Non-BCS-type superconductivity and critical thickness of $SrTiO_3/LaAlO_3/SrTiO_3$ trilayer interface system

Yongsu Kwak [a,b,1], Woojoo Han [a,c,1], Thach D.N. Ngo [a], Dorj Odkhuu [d], Young Heon Kim [e], Sonny H. Rhim [f], Mahn-Soo Choi [g], Yong-Joo Doh [h], Joon Sung Lee [i], Jonghyun Song [b,j,*], Jinhee Kim [a,*]

[a] Korea Research Institute of Standards and Science, Daejeon 34113, Republic of Korea
[b] Department of Physics, Chungnam National University, Daejeon 34134, Republic of Korea
[c] Department of Nanoscience, University of Science and Technology, Daejeon 34113, Republic of Korea
[d] Department of Physics, Incheon National University, Incheon 22012, Republic of Korea
[e] Graduate School of Analytical Science and Technology, 99 Daehak-ro, Yuseong-gu, Daejeon 34134, South Korea
[f] Department of Physics and Energy Harvest Storage Research Center (EHSRC), University of Ulsan, Ulsan 44610, Republic of Korea
[g] Department of Physics, Korea University, Seoul 02841, Republic of Korea
[h] Department of Physics and Photon Science, Gwangju Institute of Science and Technology, Gwangju 61005, Republic of Korea
[i] Display and Semiconductor Physics, Korea University Sejong Campus, Sejong 30019, Republic of Korea
[j] Institute of Quantum Systems (IQS), Chungnam National University, Daejeon 34134, Republic of Korea

ARTICLE INFO

Keywords:
$SrTiO_3$-capped $LaAlO_3$
$SrTiO_3$ or $SrTiO_3$
$LaAlO_3$
$SrTiO_3$ trilayer
Critical thickness
two-dimensional electron gas (2DEG)
Superconductivity
Non-BCS-type

ABSTRACT

As a quest for two-dimensional conducting interface with exotic functionalities for future electronic devices, the perovskite heterointerface of $LaAlO_3/SrTiO_3$ (LAO/STO) has been intensively studied. For the LAO/STO heterostructure, the critical thickness of the LAO layer for metallic conduction is 4 unit cells (uc) according to the polar catastrophe scenario. However, we find that metallic conduction can also be induced at the LAO/STO interface with only 1 uc of LAO, as long as it is capped by 3 or more uc of STO. Consistent results are obtained from density functional theory calculations. For this STO/LAO/STO trilayer, we also confirmed a peculiar non-BCS-type superconductivity with a suppressed superconducting gap, which may imply a superconducting coupling distinct from previously reported BCS-type superconductivity in LAO/STO heterointerface. These observations suggest that the STO/LAO/STO trilayer can be another testing board to explore carrier conduction in two-dimensional electron systems for electronic device applications utilizing exotic functionalities.

1. Introduction

Since its discovery by Ohtomo and Hwang in 2004 [1], the two-dimensional electron gases (2DEGs) formed at the interface between the band insulators $LaAlO_3$ (LAO) and $SrTiO_3$ (STO) have attracted great interest. Besides the striking formation of 2DEGs, various properties including Rashba spin–orbit coupling [2,3], ferromagnetism [4,5], and superconductivity [6] were also reported from this heterostructure system. Some scenarios involving oxygen vacancies [7], cationic interdiffusion [8], a polar catastrophe [9,10] have been suggested for researchers to understand the origin of the 2DEGs formed at the heterointerface between the two different band insulators of $LaAlO_3$ and $SrTiO_3$. The polar catastrophe scenario explains the emergence of 2DEGs by an electronic reconstruction (transfer of negative charges from the LAO surface to the embedded interface), which prevents the divergence of electrostatic potential built up by layer-by-layer addition of the alternating polar LaO and AlO_2 slabs on the TiO_2 terminated STO(1 0 0) substrate. This scenario requires that the LAO thickness is equal to or larger than 4 unit cells (uc), so that an overlap occurs between the conduction band of the surface LAO layer and the valence band of the interface STO to enable the charge transfer for the electronic reconstruction. For the 'critical' thickness of LAO (4 uc), there have been efforts to reduce it by capping surface with various metals [11–13].

Two-dimensional interfacial conduction between metallic

* Corresponding authors at: Department of Physics, Chungnam National University, Daejeon 34134, Republic of Korea (J. Song).
E-mail addresses: songjonghyun@cnu.ac.kr (J. Song), jinhee@kriss.re.kr (J. Kim).
[1] Authors contributed equally

https://doi.org/10.1016/j.apsusc.2021.150495
Received 26 March 2021; Received in revised form 7 June 2021; Accepted 25 June 2021
Available online 28 June 2021

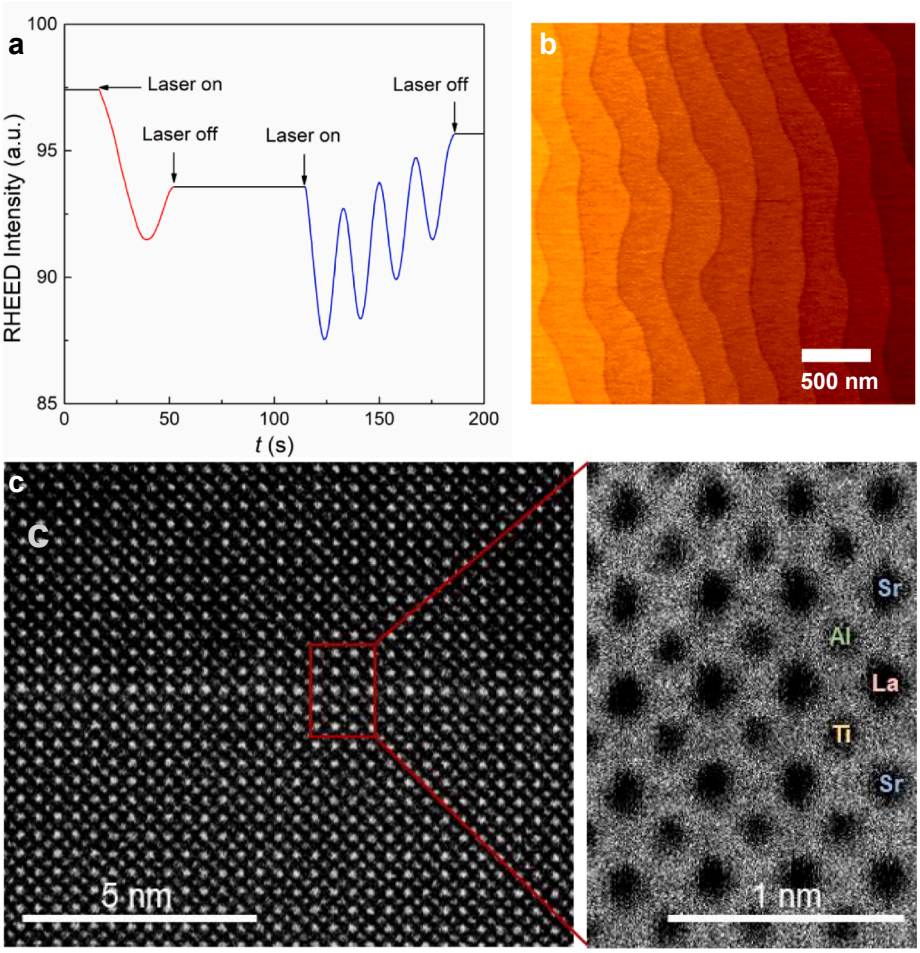

Fig. 1. (a) RHEED intensity of $(SrTiO_3)_4/(LaAlO_3)_1/SrTiO_3$. Red line shows one-unit cell of $LaAlO_3$ and blue line shows four-unit cell of $SrTiO_3$. (b) AFM image of the trilayer system. (c) Cross-sectional HR-TEM image for $(SrTiO_3)_{30}/(LaAlO_3)_1/SrTiO_3$. A one unit-cell-thick $LaAlO_3$ stands out from the $SrTiO_3$ background of the substrate and the capping layer. (For interpretation of the references to colour in this figure legend, the reader is referred to the web version of this article.)

perovskites was also reported in STO/LAO/STO triple-layered system, which provides an alternative to the LAO/STO [14–16]. The interface conduction appears after depositing a capping STO on LAO/STO even when the thickness of the LAO layer is less than 4 uc. The common observation in these reports is the parallel two-dimensional conducting channels, unlike what is observed from uncapped LAO/STO, consisting of electron- and hole-type carriers at the two different interfaces: electron conduction at the interface of LAO and STO substrate (LaO/TiO_2) and hole conduction at the interface between the LAO and the STO capping layer (SrO/AlO_2). However, there is discrepancy in the minimally required thickness of the sandwiched LAO layer for the onset of metallic conduction. Huijben *et al.* observed the metallic conductivity even from sample with a 1-uc-thick LAO layer [14] whereas other studies [15,16] reported that at least a 2- or 3-uc-thick LAO layer is needed to induce the accumulation of carriers at the interfaces. Also, about the origin of observed metallicity, it was suggested that the polar discontinuity, accompanying the shift of the O 2*p* states and expanded dispersive O 2*p* surface state trigger the electronic reconstruction [15]. Recently, however, Su *et al.* suggested head-to-head polarization, arising from the strain-field interference due to the tensile strain at the bottom interface and a parasitic flexoelectriclike effect exerted onto the top counterpart [17].

As mentioned above, although there have been such reports on the trilayer STO/LAO/STO with LAO slabs with a thickness larger than 2-uc, focused study on the same system but with extremely thin (1 uc) LAO is absent up to now. Moreover, the superconducting property of this 'triple structure' has never been reported to our knowledge. In this work, we studied electronic transport properties of LAO/STO capped with STO. Even though the LAO layer is thinner than the critical thickness, 4 uc, interface conduction in this trilayer system occurs if the total thickness of the LAO and STO films equals or exceeds 4 uc even with a 1-uc-thick LAO layer. Additionally, we studied the superconductivity in LAO/STO capped with STO by investigating the supercurrent transport in a vertical superconducting tunnel junction with an Al counter electrode. We found that this trilayer system exhibits superconductivity, and the temperature dependence of the superconducting energy gap does not follow BCS theory. Our results not only contribute to the study of reducing the critical thickness of LAO less than 4 uc in LAO/STO, but also suggest that two-dimensional electron system in trilayer STO/LAO/STO may be another conducting interface with yet unexplored functionalities.

2. Materials and methods

2.1. Preparation of the STO/LAO/STO trilayer

TiO_2-terminated $SrTiO_3$ (STO) substrate was prepared by selectively etching SrO by using buffered oxide etch. Before film growth, the STO substrates were annealed at 950 °C under an oxygen pressure of 2×10^{-5} Torr for 2 h. $LaAlO_3$ (LAO) film of 1–4 uc and then STO capping layers of 1–10 uc were deposited on the STO substrate at 750 °C under an oxygen pressure of ~ 10^{-5} Torr. The laser pulse energy was 120 mJ with a repetition rate of 1 Hz. After growth, the samples were annealed in situ in an oxygen-rich atmosphere (500 mTorr) at 750 °C for 30 min and then

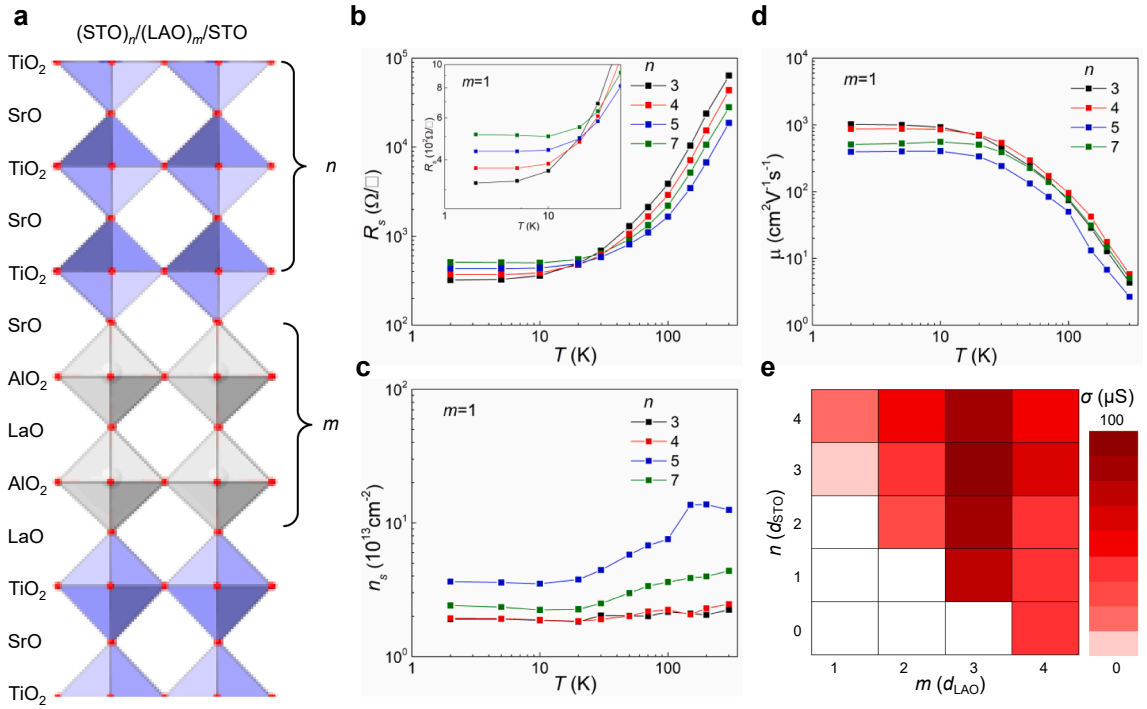

Fig. 2. (a) Schematic atomic structures of $(SrTiO_3)_n/(LaAlO_3)_m/SrTiO_3$. Blue(gray) octahedral represents $SrTiO_3(LaAlO_3)$. Small red spheres at the vertices of the octahedron are oxygen atoms. For simplicity, cations and the bottom two unit cells of $SrTiO_3$ substrate are not shown. (b) Temperature dependence of sheet resistance for $(SrTiO_3)_n/(LaAlO_3)_1/SrTiO_3$. Inset is a zoomed graph at low temperature. (c) and (d) Temperature dependences of carrier density and mobility for $(SrTiO_3)_n/(LaAlO_3)_1/SrTiO_3$. (e) Conductivity of the interface at room temperature as a function of the thickness of the $LaAlO_3(m)$ and $SrTiO_3(n)$ layers. (For interpretation of the references to colour in this figure legend, the reader is referred to the web version of this article.)

cooled to room temperature under the same oxygen pressure.

2.2. Fabrication of superconducting tunnel junction

A Hall bar pattern with dimensions of 5 μm × 20 μm was lithographically defined on the $(STO)_7/(LAO)_1/STO$ trilayer. To prevent probable current leakage, the edges of the conducting interface in this heterostructure were covered by hardened PMMA (polymethyl methacrylate). An Al (140 nm)/Ti (10 nm) top electrode was then deposited on the oxide Hall bar by rf sputtering to make a vertical superconducting tunnel junction.

2.3. Electrical transport measurements

The temperature-dependent sheet resistance of the unpatterned trilayer samples was measured using the van der Pauw method (Quantum Design PPMS). For experiments on the superconducting tunnel junction, we used a dilution refrigerator to measure the superconducting energy gap of the trilayer. We measured *I*–*V* and d*I*/d*V*–*V* for the interface channel and the tunnel junction by using the conventional four-point dc and ac technique.

2.4. Density functional calculations

Density functional theory (DFT) simulations were performed using Vienna ab initio simulation package (VASP) [18] with generalized gradient approximation (GGA) for the exchange correlation potential in projector augmented-wave basis. Experimental lattice constant (0.3905 nm) of STO was used for the in-plane lattice in calculations. Considering the coherent in-plane lattice constant of LAO slab (~0.379 nm) to that of STO revealed by transmission electron microscopy measurement in Fig. 1c, the sandwiched LAO layer is subjected to tensile strain due to lattice mismatch. Dipole corrections were included to eliminate any artificial electric field across due to supercell configurations. Energy cutoff of 600 eV and a 15 × 15 × 1 k-point grid are used where force criteria of 10–2 eV/Å is employed for atomic relaxations

3. Results and discussion

LAO and STO layers of various thickness were grown on TiO_2-terminated STO substrates. The layer thickness was controlled by observing reflection high-energy diffraction (RHEED) patterns during growth. Fig. 1a is RHEED intensity graph showing that the LAO and STO layers were deposited in a layer-by-layer growth mode. As shown in the AFM image of Fig. 1b, the final trilayer surface was smooth and fine with wide terraces. Fig. 1c is high-angle annular dark-field and annular bright-field scanning transmission electron microscopy images of $(STO)_{30}/(LAO)_1/STO$ sample. The 1-uc-thick LAO film can be seen clearly, with the La atoms standing out from the array of Sr atoms. It appears that the LAO film is fully strained, and that the interfaces are atomically sharp and free of defects such as misfit dislocations.

We investigated the electrical transport property of the $(STO)_n/(LAO)_m/STO$ samples measured by the van der Pauw method, and its dependence on the number of unit cells *n* and *m* (see Fig. 2a). Fig. 2b is the temperature dependence of the sheet resistance(R_s) of $(STO)_n/(LAO)_1/STO$ trilayer samples with $m = 1$ (1 uc LAO). All the samples showed metallically decreasing resistance as the temperature was lowered. Noticeably, the samples with mere 1 uc of LAO layer ($m = 1$), though it is far thinner than the well-known critical thickness of 4 uc for the LAO/STO heterostructure, exhibits electrical conduction as long as the thickness of the capping STO layer is 3 uc or above. In previous works, similar results were reported; STO/LAO/STO trilayer samples showed electrical conductivity even when the LAO thickness was less than 4 uc [15,16]. However, we observed metallic conduction even in samples with an extremely thin LAO layer (1 uc) as shown in Fig. 2b, whereas insulating property was reported for similar circumstances in

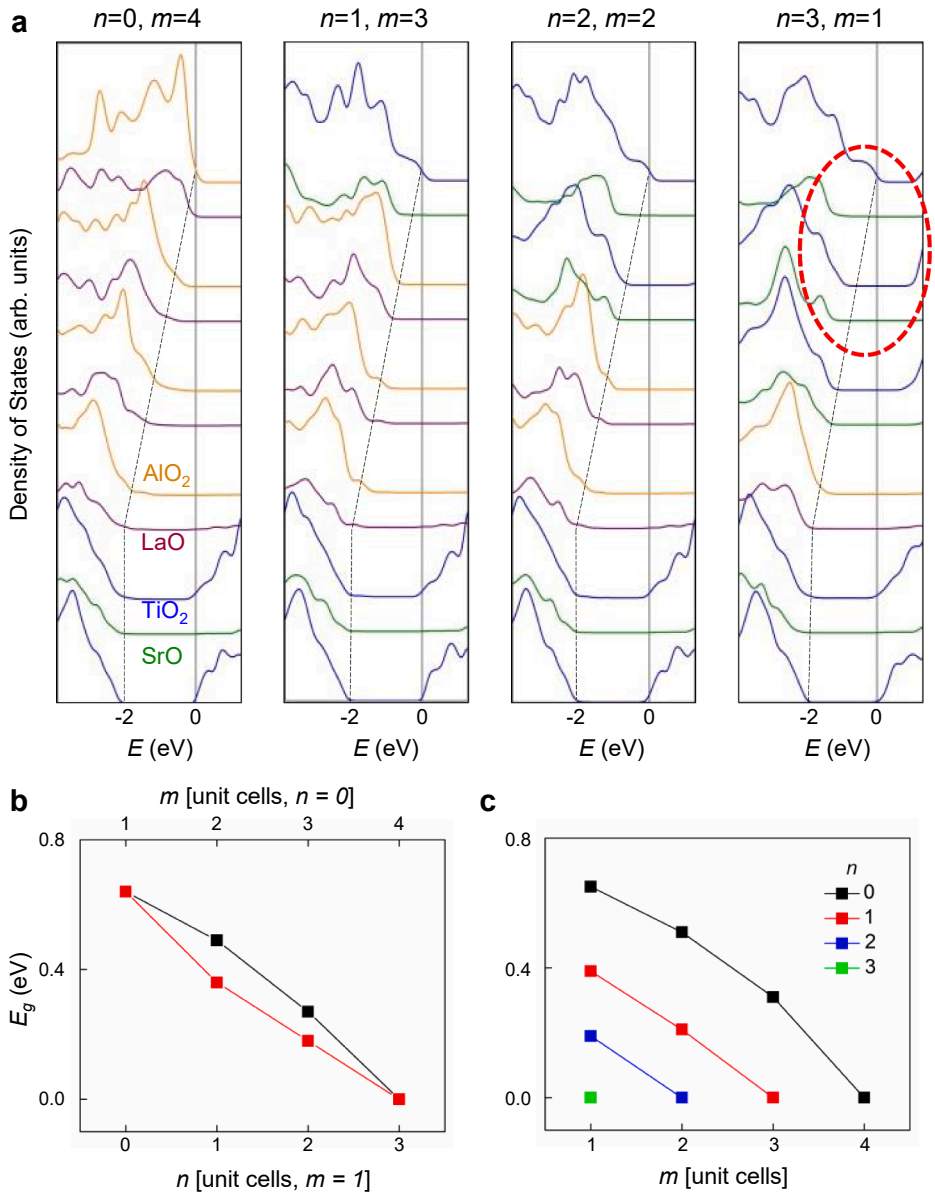

Fig. 3. (a) Layer-resolved density of state (DOS) for $(SrTiO_3)_n/(LaAlO_3)_m/SrTiO_3$ referenced at the bottom of the Ti 3*d* band at the interface. (b) Comparison of bandgap energy for $(SrTiO_3)_n/(LaAlO_3)_1/SrTiO_3$ and $(LaAlO_3)_m/SrTiO_3$. (b) Comprehensive picture for bandgap energy, E_g, for $(SrTiO_3)_n/(LaAlO_3)_m/SrTiO_3$ as function of n and m.

the previous works. This observation is surprising since it indicates that sandwiching only two alternating polar slabs in LAO induces a two-dimensional metallic channel.

In addition, the thickness dependence of the sheet resistance at low temperature is notable: R_s at relatively high temperatures, which is not well-ordered respect to the number n of the STO capping layers, becomes ordered below $T \sim 10$ K with an inverse tendency exhibiting a lowest value for the thinnest STO ($n = 3$) as shown in the inset of Fig. 2b. This result indicates that the conductivity of two-dimensional metallic channel becomes optimal at low temperature with lowering the thickness of STO capping layer and also implies lowering the thickness of STO capping layer affects the carrier density(n_s) and mobility(μ). Fig. 2c and Fig. 2d show the temperature dependences of n_s and μ of $(STO)_n/(LAO)_1/STO$ with different STO capping layer thickness n, extracted from Hall measurements and sheet resistances. As shown, each n_s and μ are not ordered with respect to n due to especially the sample of $n = 5$. Considering the fact of $R_s = 1/qn_s\mu$ of where q is charge of a carrier, the overall shape of the R_s–T curves in Fig. 2d is dominated by the μ rather than n_s since the overall shape of temperature dependences of inverse μ (μ^{-1}-T curves) is similar to the R_s–T curves. However, the reordering of R_s with respect to n at low temperature (see the inset of Fig. 2b) is attributed to the temperature dependency of n_s as shown in Fig. 2c whereas its origin is unclear in current: the most rapidly decreased n_s with decreasing the temperature for the sample of $n = 5$ (the next is $n = 7$, see Fig. 2c) and the observed almost similar ratio of μ between the different n in the measured temperature range (see Fig. 2d) reorder the values of R_s ($\sim 1/n_s\mu$) with respect to n at low temperature. Further study is needed to elucidate the exact origin of the behavior of n_s with respect to temperature.

To obtain a comprehensive picture about the onset of conduction, we assessed the room-temperature electrical conductivity of the $(STO)_n/(LAO)_m/STO$ trilayer samples as a function of m and n. As shown in Fig. 2e, we find that the trilayer system becomes conductive when $m + n \geq 4$. For example, in the case of $m = 2$, the trilayer system is conductive only when n is 2 or higher. When the total film thickness is less than 4, we could not observe metallic conduction for the any combination of m

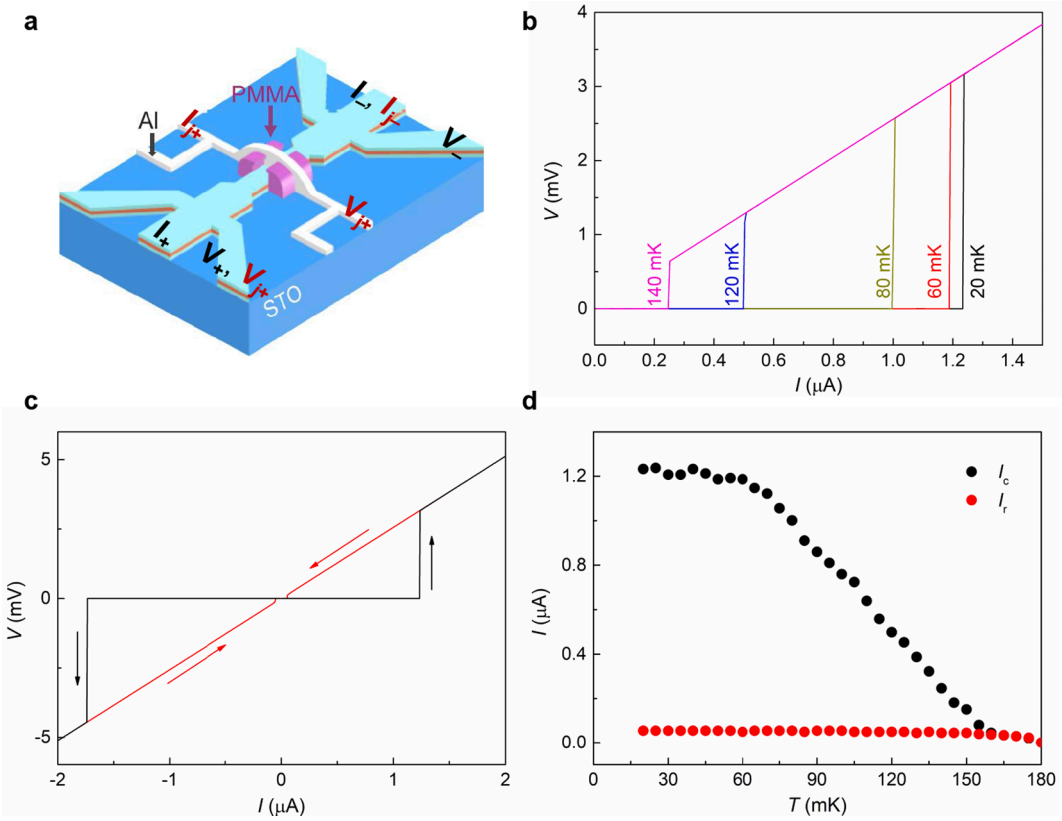

Fig. 4. (a) Schematic of the Al/Ti/$(SrTiO_3)_7$/$(LaAlO_3)_1$/$SrTiO_3$ tunnel junction. In four-probe measurement for the two-dimensional interface (the Josephson junction), current is applied from I_+ to I_- (from I_{j+} to I_{j-}) and voltage is simultaneously measured between V_+ and V_- (between V_{j+} and V_{j-}). (b) The evolution of *I-V* characteristic curve of the oxide interface with temperature. (c) *I-V* characteristic curve of two dimensional interface channel by sweeping the current at $T = 20$ mK. Arrows indicate the sweep direction of current bias. (d) Temperature dependence of the superconducting critical current, (I_c, black filled circle) and the return current, (I_r, red filled circle) for positive polarity in $(SrTiO_3)_7$/$(LaAlO_3)_1$/$SrTiO_3$. (For interpretation of the references to colour in this figure legend, the reader is referred to the web version of this article.)

(LAO) and n (STO). Our findings about the LAO and STO capping layer thickness are summarized as follows: (i) $m + n \geq 4$ is a prerequisite to triggers the observed carrier doping at the interface and (ii) metallic conduction occurs also in samples with mere 1-uc-thick LAO.

Our experimental observations were confirmed by theoretical calculations. Fig. 3a is the layer-resolved density of states of LAO/STO and STO/LAO/STO. These results indicate that the STO capping impacts dramatically on the electronic structure of LAO/STO. For the LAO/STO heterostructure ($n = 0$, $m = 4$), the O 2*p* state in the LAO film gradually shifts towards the Fermi energy as getting closer to the surface. As a result, the band gap decreases with increasing LAO thickness and eventually vanishes when it reaches 4 uc (Fig. 3a and 3c), consistent with a previous study [19]. For the 4-uc LAO layer ($m = 4$), charge transfer occurs from the surface AlO_2 into the interface Ti d_{xy}, which induces fractional occupation of t_{2g} orbital states of the Ti^{3+} ($3d^1$) state. This supports the well-known polar catastrophe scenario, and explains the experimental result for $m = 4$. Note that the band gap of STO in the calculated density of states is smaller than 3.2 eV of the experiment due to the well-known underestimation of band gap in DFT. For the $(STO)_n$/$(LAO)_m$/STO trilayer, theoretical calculation shows that O 2*p* state of TiO_2 slabs in the STO capping layers also shifts upward as they approach to the surface. This unexpected valence band shift in nonpolar STO slabs, although the shift is slower than in LAO (see the dotted circle in Fig. 3a), originates from the presence of built–in potential within STO layer, which stems from buckling by atomic relaxations. The 1-uc-LAO on STO substrate is insulating (see Fig. 3c, $n = 0$), but the bandgap disappears after adding 3 uc or more of STO capping layers (Fig. 3b and 3c), as in LAO/STO. Here, it should be noted that the O 2*p* state of the TiO_2 surface slab shift significantly towards the Fermi energy compared to the state at the subsurface (see upper side in the dotted circle in Fig. 3a). This is attributed to the expanded O 2*p* surface state which is analogous to the one on the clean STO(0 0 1) surface [20,21]. Eventually, the electron transfer from O 2*p* of the surface to the interface Ti d_{xy} is enabled by STO capping, resulting in an insulator-to-metal transition. In addition, Fig. 3b shows that the band gaps of $(STO)_n$/$(LAO)_1$/STO with a total thickness of 4 uc or less are similar but slightly smaller than those of corresponding $(LAO)_{n+1}$/STO. Closing of band gap is found in DFT calculation when the total thickness of the LAO and STO capping layers, $m + n$, is 4 uc. This result is consistent with the experimental result shown in Fig. 2e.

For further investigation of the trilayer system, we made a Josephson junction device using $(STO)_7$/$(LAO)_1$/STO. A Hall bar-type mesa was fabricated by using photolithography and Ar-ion milling for investigating whether the oxide interface exhibits superconductivity at low temperatures (see Fig. 4a). Additionally, a vertical tunnel junction was integrated in the device by depositing a Ti (10 nm)/Al (140 nm) superconducting electrode in a cross-strip configuration, and information on the superconducting energy gap of $(STO)_7$/$(LAO)_1$/STO was obtained. As shown in Fig. 4b, at temperatures below $T_c = 180$ mK, the two-dimensional channel resistance drops to zero, and the current–voltage (*I-V*) characteristic curves show a superconducting state. The superconducting critical temperature of $(STO)_7$/$(LAO)_1$/STO is comparable with those of typical LAO/STO heterostructures [6]. Fig. 4c shows the *I-V* characteristic curve measured at $T = 20$ mK, where the critical currents are asymmetric for positive and negative polarities. Considering the possibility of coexistence ferromagnetism and superconductivity in our samples, as in the case of LAO/STO heterostructure [22,23], the asymmetric *I-V* characteristic can be attributed to the

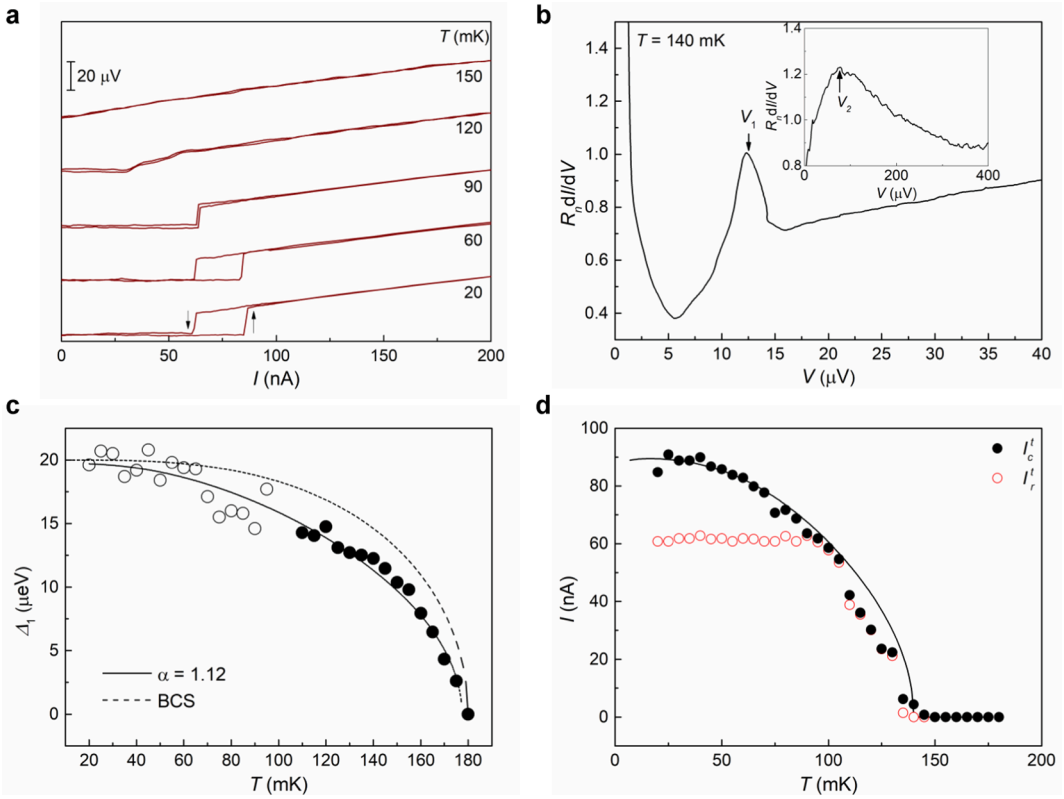

Fig. 5. (a) Temperature-dependent *I–V* characteristics of the Al/Ti/$(SrTiO_3)_7$/$(LaAlO_3)_1$/$SrTiO_3$ tunnel junction. (b) The d*I*/d*V*–*V* curve of the tunnel junction at 140 mK, showing a clear peak at the voltage of 12 μV. The inset provides a clear peak at 78 μV. (c) Temperature dependence of the superconducting energy gap of the interface superconductor Δ_1, estimated from the voltage jump in the *I–V* curve (open circle) and from the peak position in the d*I*/d*V*–*V* curve (filled circle). The solid line is the best fit to an empirical formula with $\alpha = 1.12$ and $\Delta_1(0)/k_BT_c = 1.31$, while the dashed line is a fit to the BCS formula with $\alpha = 1.74$. (d) Temperature dependence of the critical current (I_c^t, filled circle) and the retrapping current (I_r^t, open circle) of the tunnel junction. The solid line is a fit to the Ambegaokar–Baratoff relation.

ferromagnetic feature of our trilayer [24]. At the temperature below 155 mK, the *I-V* curve is hysteretic; at $T = 20$ mK, the critical current and the return current for positive polarity are $I_c = 1.2$ μA and $I_r = 55$nA, respectively (See Fig. 4c). Fig. 4d shows that the critical current for positive polarity decreases with increasing temperature, while the return current for positive polarity has almost no temperature dependence up to $T = 155$ mK. The critical current becomes identical to the return current above $T = 155$ mK.

Fig. 5a is a set of representative *I-V* curves of the tunnel junction measured at various temperatures. At temperatures below 150 mK, the *I-V* curve at the tunnel junction shows a superconducting state, and a resistive state is presumably from the tunneling of quasi-particles. Note that the junction critical current (I_c^t) is much lower than the critical current (I_c) of the patterned two-dimensional channel of $(STO)_7$/$(LAO)_1$/STO. At $T = 20$ mK, the junction critical current and the normal resistance are $I_c^t = 85$nA and $R_n = 140$ Ω, respectively. The hysteresis shown in the *I-V* curves is typical of capacitively coupled Josephson junctions.

Fig. 5b shows the differential conductance of the tunnel junction as a function of the junction voltage at $T = 140$ mK. Above $T = 110$ mK, two conductance peaks are observed in the quasi-particle branch. One of the conductance peaks appears at $V_1 = 12$ μV and another at $V_2 = 78$ μV (see inset). Conductance peaks in the quasi-particle branch of a Josephson junction gives information about the energy gap of the superconductors consisting the tunnel junction. For a superconductor/insulator/superconductor (S/I/S′) asymmetric Josephson junction of which the two superconductors have different superconducting energy gaps, Δ_1 and Δ_2, quasiparticle tunneling peaks in the differential conductance curve will appear at the bias voltages of $|\Delta_1 - \Delta_2|/e$ and $(\Delta_1 + \Delta_2)/e$. Considering that the superconducting energy gap of Al is about 100 ~ 120 μeV, it is impossible to explain the appearance of two conductance peaks at the same time. On the other hand, if the sample is modeled by a superconductor/normal/superconductor (S/N/S′) asymmetric Josephson junction, the two peaks can be explained by Andreev reflections between the Al electrode and the oxide interface. This suggests that our tunnel junction is a S/N/S′ asymmetric Josephson junction.

For an S/N/S′ asymmetric Josephson junction, a series of peaks attributed to multiple Andreev reflections can be observed from d*I*/d*V* measurements [25,26]. It appears that only the lowest order reflections are observed in our case. Assuming that the two conductance peaks represent the superconducting gap energies, by $V_1 = \Delta_1/e$ and $V_2 = \Delta_2/e$, we obtained the temperature dependence of Δ_1 from the peak voltage of the d*I*/d*V*-*V* curve from $T = 110$ mK to 180 mK. However, at temperatures below 100 mK, we estimated Δ_1 from the voltage jump in the *I-V* curves, since the conductance peaks indicating Δ_1 were not observed. The reason for estimating Δ_1 from the voltage jump was specified in Appendix A. Fig. 5c shows a temperature dependence of Δ_1 from the voltage jumps in the *I–V* curves (open circle) and the peak voltages of the d*I*/d*V*–*V* curves (filled circle). Fitting the data to the empirical formula $\Delta_1(T) = \Delta_1(0)\tanh[\alpha(T_c/T-1)^{1/2}]$ gives $\alpha = 1.12$ (solid line), which deviates from $\alpha = 1.74$ (dashed) expected from BCS theory. The measured I_c^t data fit well to the Ambegaokar-Baratoff [27] relation adopting the non-BCS-type $\Delta_1(T)$ for the interface superconductor and a BCS-type $\Delta_2(T)$ for Al as shown in Fig. 5d. In addition, we measured the magnetic field dependence of I_c^t by measuring *I-V* curves in the applied magnetic field ranged from −60 mT to −60 mT. In these measurements, we observed Fraunhofer pattern confirming the Josephson junction.

As a final remark, we comment on the observed nontrivial superconductivity in STO capped LAO/STO heterointerface. The value of $\Delta/k_BT_c = 1.31$ obtained from Fig. 5c is definitely lower than the

canonical BCS model value of 1.76, whereas a value confirming to the BCS model, $\Delta/k_BT_c \sim 1.7$, was reported for the bare LAO/STO [28]. This result along with the numerical analysis results discussed above obviously indicates that the superconductivity of STO-capped LAO/STO is 'non-BCS-type' with much weaker coupling, which is different from the normal BCS-type weakly coupled superconductivity of LAO/STO [29]. In fact, the Δ/k_BT_c in LAO/STO [28] was measured by using the 'planar' structured N/S junction device which was different to our device. There may be concerns about variations in Δ/k_BT_c depending on the geometry of device. In fabrication process for the planar structured N/S junction, Ar-ion etching which may generate oxygen vacancy was included to connect the normal metal to superconducting 2DEGs in LAO/STO. On the other hands, our device consist of vertical tunnel junctions is free from the oxygen vacancy since the Ti and Al layers were only deposited vertically on the capping STO layer without an etching process. Therefore, we believed that the vertical tunnel junction gives more accurate information on Δ/k_BT_c. In addition to our results, non-BCS-type superconductivity with a suppressed gap has been reported for uncapped (1 1 0)-oriented LAO/STO interface [30]. The gap suppression is attributed to a Lifshitz transition induced by electrostatic gating, which populates a second band and turns the system from a BCS-type single-condensate superconductor to a two-condensate superconductor. However, such a Lifshitz transition was not observed in our STO/LAO/STO trilayer system. These observations indicate that the electrical conduction in STO/LAO/STO has different nature from that of bare LAO/STO. The detailed analysis and interpretation on the electrical-transport in STO-capped LAO/STO will be reported elsewhere.

4. Conclusions

In this work, we have demonstrated experimentally and theoretically that an electrical conduction channel is introduced in the STO/LAO/STO system when the total thickness of the LAO and the STO capping layer equals or exceeds 4 uc, and that the conduction is associated with charge transfer from the STO surface to the interface. Electrical-transport measurements showed that the interface electron system of the STO/LAO/STO formed a superconducting phase below $T = 180$ mK. We obtained the superconducting energy gap of STO/LAO/STO from electrical-transport measurements, and found that the temperature dependence of the superconducting energy gap with suppressed superconducting energy gap did not follow BCS theory. The vastly weak-coupled superconductivity of STO/LAO/STO, suggested from our results, is peculiar in comparison with the BCS-type superconductivity reported from bare LAO/STO. The STO/LAO/STO trilayer system can be a new testing ground for investigating unconventional superconductivity at oxide interfaces.

CRediT authorship contribution statement

Yongsu Kwak: Methodology, Formal analysis. **Woojoo Han:** Methodology, Formal analysis. **Thach D.N. Ngo:** Writing - original draft. **Dorj Odkhuu:** Formal analysis. **Young Heon Kim:** Methodology. **Sonny H. Rhim:** Formal analysis. **Mahn-Soo Choi:** Conceptualization. **Yong-Joo Doh:** Conceptualization. **Joon Sung Lee:** Conceptualization, Supervision. **Jonghyun Song:** Supervision. **Jinhee Kim:** Resources, Supervision.

Declaration of Competing Interest

The authors declare that they have no known competing financial interests or personal relationships that could have appeared to influence the work reported in this paper.

Acknowledgments

This work was supported by Korea Institute for Advancement of Technology(KIAT) grant funded by the Korea Government(MOTIE) (P0008458, The Competency Development Program for Industry Specialist), Basic Science Research Program through the National Research Foundation of Korea(NRF) funded by the Ministry of Education(NRF-2020R1A6A1A03047771, NRF-2019R1I1A3A01059880), the Max Planck POSTECH/Korea Research Initiative, Study for Nano Scale Optomaterials and Complex Phase Materials (2016K1A4A4A01922028), though NRF funded by MSIP of Korea, NRF grant funded by MSIP (2020R1A2C1011000, 2016R1A5A1008184).

Appendix A. Supplementary material

Supplementary data to this article can be found online at https://doi.org/10.1016/j.apsusc.2021.150495.

References

[1] A. Ohtomo, H.Y. Hwang, A high-mobility electron gas at the $LaAlO_3/SrTiO_3$ heterointerface, Nature 427 (2004) 423–426, https://doi.org/10.1038/nature02308.
[2] A.D. Caviglia, M. Gabay, S. Gariglio, N. Reyren, C. Cancellieri, J.-M. Triscone, Tunable Rashba Spin-Orbit Interaction at Oxide Interfaces, Phys. Rev. Lett. 104 (2010), 126803, https://doi.org/10.1103/PhysRevLett.104.126803.
[3] J.-W. Chang, J. Song, J.S. Lee, H. Noh, S.K. Seung, L. Baasandorj, S.G. Lee, Y.-J. Doh, J. Kim, Quantum Electrical Transport in Mesoscopic $LaAlO_3/SrTiO_3$ Heterostructures, Appl. Phys. Express. 6 (2013) 85201, https://doi.org/10.7567/apex.6.085201.
[4] X. Ariando, G. Wang, Z.Q. Baskaran, J. Liu, J.B. Huijben, A. Yi, A.R. Annadi, A. Barman, S. Rusydi, Y.P. Dhar, J. Feng, H. Ding, T. Hilgenkamp, Venkatesan, Electronic phase separation at the $LaAlO_3/SrTiO_3$ interface, Nat. Commun. 2 (2011) 188, https://doi.org/10.1038/ncomms1192.
[5] T.D.N. Ngo, J.-W. Chang, K. Lee, S. Han, J.S. Lee, Y.H. Kim, M.-H. Jung, Y.-J. Doh, M.-S. Choi, J. Song, J. Kim, Polarity-tunable magnetic tunnel junctions based on ferromagnetism at oxide heterointerfaces, Nat. Commun. 6 (2015) 8035, https://doi.org/10.1038/ncomms9035.
[6] N. Reyren, S. Thiel, A.D. Caviglia, L.F. Kourkoutis, G. Hammerl, C. Richter, C.W. Schneider, T. Kopp, A.-S. Rüetschi, D. Jaccard, M. Gabay, D.A. Muller, J.-M. Triscone, J. Mannhart, Superconducting Interfaces Between Insulating Oxides, Science (80-.). 317 (2007) 1196 LP – 1199. https://doi.org/10.1126/science.1146006.
[7] A. Kalabukhov, R. Gunnarsson, J. Börjesson, E. Olsson, T. Claeson, D. Winkler, Effect of oxygen vacancies in the $SrTiO_3$ substrate on the electrical properties of the $LaAlO_3/SrTiO_3$ interface, Phys. Rev. B. 75 (2007), 121404, https://doi.org/10.1103/PhysRevB.75.121404.
[8] P.R. Willmott, S.A. Pauli, R. Herger, C.M. Schlepütz, D. Martoccia, B.D. Patterson, B. Delley, R. Clarke, D. Kumah, C. Cionca, Y. Yacoby, Structural Basis for the Conducting Interface between $LaAlO_3/SrTiO_3$, Phys. Rev. Lett. 99 (2007), 155502, https://doi.org/10.1103/PhysRevLett.99.155502.
[9] N. Nakagawa, H.Y. Hwang, D.A. Muller, Why some interfaces cannot be sharp, Nat. Mater. 5 (2006) 204–209, https://doi.org/10.1038/nmat1569.
[10] S. Thiel, G. Hammerl, A. Schmehl, C.W. Schneider, J. Mannhart, Tunable Quasi-Two-Dimensional Electron Gases in Oxide Heterostructures, Science (80-.). 313 (2006) 1942 LP–1945. https://doi.org/10.1126/science.1131091.
[11] E. Lesne, N. Reyren, D. Doennig, R. Mattana, H. Jaffrès, V. Cros, F. Petroff, F. Choueikani, P. Ohresser, R. Pentcheva, A. Barthélémy, M. Bibes, Suppression of the critical thickness threshold for conductivity at the $LaAlO_3/SrTiO_3$ interface, Nat. Commun. 5 (2014) 4291, https://doi.org/10.1038/ncomms5291.
[12] D.C. Vaz, E. Lesne, A. Sander, H. Naganuma, E. Jacquet, J. Santamaria, A. Barthélémy, M. Bibes, Tuning Up or Down the Critical Thickness in $LaAlO_3/SrTiO_3$ through In Situ Deposition of Metal Overlayers, Adv. Mater. 29 (2017) 1700486, https://doi.org/10.1002/adma.201700486.
[13] Y. Zhou, P. Wang, Z.Z. Luan, Y.J. Shi, S.W. Jiang, H.F. Ding, D. Wu, Patterning the two dimensional electron gas at the $LaAlO_3/SrTiO_3$ interface by structured Al capping, Appl. Phys. Lett. 110 (2017), 141603, https://doi.org/10.1063/1.4979784.
[14] M. Huijben, G. Rijnders, D.H.A. Blank, S. Bals, S. Van Aert, J. Verbeeck, G. Van Tendeloo, A. Brinkman, H. Hilgenkamp, Electronically coupled complementary interfaces between perovskite band insulators, Nat. Mater. 5 (2006) 556–560, https://doi.org/10.1038/nmat1675.
[15] R. Pentcheva, M. Huijben, K. Otte, W.E. Pickett, J.E. Kleibeuker, J. Huijben, H. Boschker, D. Kockmann, W. Siemons, G. Koster, H.J.W. Zandvliet, G. Rijnders, D.H.A. Blank, H. Hilgenkamp, A. Brinkman, Parallel Electron-Hole Bilayer Conductivity from Electronic Interface Reconstruction, Phys. Rev. Lett. 104 (2010), 166804, https://doi.org/10.1103/PhysRevLett.104.166804.
[16] A.K. Singh, T.-C. Wu, M.-C. Chen, M.-Y. Song, W.-L. Lee, C.-P. Su, M.-W. Chu, Influence of $SrTiO_3$ capping layer on the charge transport at the interfaces of $SrTiO_3/LaAlO_3/SrTiO_3$ (100) heterostructure, Phys. Rev. Mater. 2 (2018), 114009, https://doi.org/10.1103/PhysRevMaterials.2.114009.
[17] C.-P. Su, A.K. Singh, T.-C. Wu, M.-C. Chen, Y.-C. Lai, W.-L. Lee, G.Y. Guo, M.-W. Chu, Impact of strain-field interference on the coexistence of electron and hole

gases in $SrTiO_3/LaAlO_3/SrTiO_3$, Phys. Rev. Mater. 3 (2019) 75003, https://doi.org/10.1103/PhysRevMaterials.3.075003.
[18] G. Kresse, J. Furthmüller, Efficiency of ab-initio total energy calculations for metals and semiconductors using a plane-wave basis set, Comput. Mater. Sci. 6 (1996) 15–50, https://doi.org/10.1016/0927-0256(96)00008-0.
[19] R. Pentcheva, W.E. Pickett, Avoiding the Polarization Catastrophe in $LaAlO_3$ Overlayers on $SrTiO_3$ through Polar Distortion, Phys. Rev. Lett. 102 (2009), 107602, https://doi.org/10.1103/PhysRevLett.102.107602.
[20] S. Kimura, J. Yamauchi, M. Tsukada, S. Watanabe, First-principles study on electronic structure of the (001) surface of $SrTiO_3$, Phys. Rev. B. 51 (1995) 11049–11054, https://doi.org/10.1103/PhysRevB.51.11049.
[21] J. Padilla, D. Vanderbilt, Ab initio study of $SrTiO_3$ surfaces, Surf. Sci. 418 (1998) 64–70, https://doi.org/10.1016/S0039-6028(98)00670-0.
[22] L. Li, C. Richter, J. Mannhart, R.C. Ashoori, Coexistence of magnetic order and two-dimensional superconductivity at $LaAlO_3/SrTiO_3$ interfaces, Nat. Phys. 7 (2011) 762–766, https://doi.org/10.1038/nphys2080.
[23] K. Michaeli, A.C. Potter, P.A. Lee, Superconducting and Ferromagnetic Phases in $LaAlO_3/SrTiO_3$ Oxide Interface Structures: Possibility of Finite Momentum Pairing, Phys. Rev. Lett. 108 (2012), 117003, https://doi.org/10.1103/PhysRevLett.108.117003.
[24] A.Y. Aladyshkin, D.Y. Vodolazov, J. Fritzsche, R.B.G. Kramer, V.V. Moshchalkov, Reverse-domain superconductivity in superconductor-ferromagnet hybrids: Effect of a vortex-free channel on the symmetry of I-V characteristics, Appl. Phys. Lett. 97 (2010) 52501, https://doi.org/10.1063/1.3474622.
[25] M. Hurd, S. Datta, P.F. Bagwell, Current-voltage relation for asymmetric ballistic superconducting junctions, Phys. Rev. B. 54 (1996) 6557–6567, https://doi.org/10.1103/PhysRevB.54.6557.
[26] U. Zimmermann, S. Abens, D. Dikin, K. Keck, V.M. Dmitriev, Multiple Andreev-reflection in asymmetric superconducting weak-links, Zeitschrift Für Phys. B Condens. Matter. 97 (1995) 59–66, https://doi.org/10.1007/BF01317588.
[27] V. Ambegaokar, A. Baratoff, Tunneling Between Superconductors, Phys. Rev. Lett. 10 (1963) 486–489, https://doi.org/10.1103/PhysRevLett.10.486.
[28] C. Richter, H. Boschker, W. Dietsche, E. Fillis-Tsirakis, R. Jany, F. Loder, L. F. Kourkoutis, D.A. Muller, J.R. Kirtley, C.W. Schneider, J. Mannhart, Interface superconductor with gap behaviour like a high-temperature superconductor, Nature 502 (2013) 528–531, https://doi.org/10.1038/nature12494.
[29] D. Rainer, J.A. Sauls, STRONG-COUPLING THEORY OF SUPERCONDUCTIVITY, in: Supercond. From Basic Phys. to Latest Dev., WORLD SCIENTIFIC, 1995: pp. 45–78. https://doi.org/doi:10.1142/9789814503891_0002.
[30] G. Singh, A. Jouan, G. Herranz, M. Scigaj, F. Sánchez, L. Benfatto, S. Caprara, M. Grilli, G. Saiz, F. Couëdo, C. Feuillet-Palma, J. Lesueur, N. Bergeal, Gap suppression at a Lifshitz transition in a multi-condensate superconductor, Nat. Mater. 18 (2019) 948–954, https://doi.org/10.1038/s41563-019-0354-z.